Mohamed *et al.*
Journal of Engineering and Applied Science (2023) 70:37
https://doi.org/10.1186/s44147-023-00195-8

Journal of Engineering and Applied Science

RESEARCH

Open Access

Modeling and simulation of short channel length effect in open drain MOSFET THz detectors

Yasmeen A. Mohamed[1*], Nihal Y. Ibrahim[2], Mohamed Y. F. El Zayat[1] and Salah E. A. Elnahwy[2]

*Correspondence:
yak00@fayoum.edu.eg

[1] Department of Physics, Faculty of Science, Fayoum University, Faiyum, Egypt
[2] Department of Engineering Physics and Mathematics, Faculty of Engineering, Cairo University, Giza, Egypt

Abstract

THz radiation detection using FET devices has attracted increasing attention lately. In this paper, we further study a simulated model of FET rectification detection in short channel length. To achieve this, both physics-based analytic model and a detailed TCAD simulation were contacted and compared. The analytical model provided detailed dependence of the response on the channel length below the extension length of the radiation. However, the simulation results were validated by comparison with the experimental data to confirm the validity of the theoretical model. These results present a new model of rectification for short channel lengths and its dependence on the extinction of AC signal through the channel.

Keywords: THz detector, Si MOSFET, Open drain mode, Channel length

Introduction

In past decades, there has been increasing interest in terahertz (THz) semiconductor radiation technology, especially field-effect transistors (FETs). FET detectors are strong candidates for THz detection. Its fast responsivity and its ability to operate at room temperature gain a lot of interest in THz detection technologies which can be used in many applications such as security, astronomy, medical imaging, scientific imaging (biochemistry, chemistry), manufacturing, and wireless communications [1–5].

At the beginning of the 1990s, Dyakonov and Shur demonstrated the possibility of application of FETs for THz technologies specially THz spectroscopy where they predicted that the output response depends on the AC fluctuations within the non-linearity of the channel [6, 7].

There are many various types of FETs, such as AlGaN/GaN high electron mobility transistors (HEMTs) [8, 9], GaAs HEMTs [10], and silicon metal–oxide–semiconductor field effect transistors (Si MOSFETs) [2, 5, 11–14], illustrated good broadband responsivities for the THz radiation [15].

According to many recent applications, silicon MOSFET is a strong candidate for THz detection with many advantages such as easy integration into electrical circuits, low production cost, and signal processing elements that can be easily combined with it.

Springer Open

© The Author(s) 2023. **Open Access** This article is licensed under a Creative Commons Attribution 4.0 International License, which permits use, sharing, adaptation, distribution and reproduction in any medium or format, as long as you give appropriate credit to the original author(s) and the source, provide a link to the Creative Commons licence, and indicate if changes were made. The images or other third party material in this article are included in the article's Creative Commons licence, unless indicated otherwise in a credit line to the material. If material is not included in the article's Creative Commons licence and your intended use is not permitted by statutory regulation or exceeds the permitted use, you will need to obtain permission directly from the copyright holder. To view a copy of this licence, visit http://creativecommons.org/licenses/by/4.0/. The Creative Commons Public Domain Dedication waiver (http://creativecommons.org/publicdomain/zero/1.0/) applies to the data made available in this article, unless otherwise stated in a credit line to the data.

Few models were developed to describe FET THz detection, such as the plasmonic response model [16, 17] the distributed resistive mixing model [11], and the non-linear R–C transmission line [18]. Lately, modeling of NQS rectification by division of a single FET to a distributed ideal FETs (BSIM3, SPICE) [19, 20] was successfully adapted, approaching more accurately the non-ideal characteristics of a transistor. Finally, the drift–diffusion transport-based models extracted the FET rectification response [21, 22] and integrated it into these basic operational equations, opening a window to more comprehensive and realistic models of FET output characteristics. The operation of the FET can be divided into two main operations: the open drain (photovoltaic) and biased (photoconductive). While the biased FET response showed increased amplification in the response, it suffered significant increase in the noise as well [23]. On the other hand, the photovoltaic operation had lower response and a much lower noise rate.

While the effect of channel length on the output response was inherently clear in the case of the biased FET, this dependence cannot be seen that clearly in the open drain case [5, 24, 25].

This is because of the direct dependence of the biased rectified response on the channel conductance, which is dependent on the channel length, while the open drain FET does not show such dependence since no current passes. Meanwhile, most models considered that the supplied AC signal decays at close proximity of one or both of the FET terminals (gate-source, and gate-drain) [24, 26]. However, in the case of an open drain, the response is independent of the channel length [21, 24].

In this work, we attempt to investigate the channel length dependence of a MOSFET operated in an open drain, and at a channel length below the ideal decay length of the input AC signal. we present in this work an analytical and a simulated model of a MOSFET as a THz detector with short channel lengths. With the help of this proposed model, we extract the response inside the transistor in an open drain condition to get a better insight into its operation and demonstrate how channel length affects transistor behavior.

The following describes how the paper is structured: The theoretical analysis and methodology of our simulation model are presented in Theoretical analysis, Methods, and Device simulation sections, respectively. The results of the simulated model are displayed in Results section, and they are discussed in Discussion section. In Conclusions section, a conclusion will be provided.

Theoretical analysis

This section develops a theoretical model for the channel length dependence on terahertz detection in short-channel FET devices (MOSFETs). The MOSFET operation in the following analysis will be considered in the open drain / linear region of operation.

The gate/source and gate/channel potentials are separated into DC (subscript 0) (V_{gs0}/V_{gc0}) and AC (subscript 1) (V_{gs1}/V_{gc1}) components, respectively under the small signal assumption. Accordingly, the AC gate/source potential V_{gs0} can be expressed as

$$V_{gs}= V_{GS} - V_{Th} = V_{gs0} + \frac{1}{2} V_{gs1}(e^{i\omega t} + e^{-i\omega t}) \tag{1}$$

where V_{GS} is the externally applied gate/source potential, and V_{gs0} is the effective DC gate/source potential such that $V_{gs0} = V_{GS0} - V_{Th}$. The gate/channel potential V_{GC} can be also written as

$$V_{GC}(x) = V_{gc0}(x) + \frac{1}{2}V_{gc1}(x)(e^{i\omega t} + e^{-i\omega t}) \tag{2}$$

where $V_{gc0} = V_{GC0} - V_{Th}$, V_{gc0} is the effective gate/channel potential. The charge continuity equation can be written as

$$\frac{\partial n}{\partial t} = \frac{1}{qW}\nabla I_c(x) \tag{3}$$

where n is the 2DEG electron density in the channel,$I_c(x)$ is the drift current through the channel, W is the depletion region width and q is The electric charge in the channel. This above equation is valid under the following gradual channel approximation,

$$n = C_g V_{gc0} \tag{4}$$

where C_g is the gate capacitance per unit area. In this case, the drift current $\mathrm{I_c(x)}$ dominates the charge flow in the channel [27],

$$I_c(x) = qn\frac{\partial V_{GC}}{\partial x} \tag{5}$$

The above equations can be separated according to [17] into:

$$\text{DC equation}: -\mu WC_g\frac{d^2}{dx^2}(\mathrm{V}_{gc0}{}^2 + \frac{1}{2}\left|\mathrm{V}_{gc1}\right|^2) \tag{6}$$

$$\text{AC equation}: -\mu WC_g\frac{d^2}{dx^2}\mathrm{V_{gc0}V_{gc1}} = \pm\frac{1}{2}i\omega C_g\mathrm{V_{gc1}} \tag{7}$$

In the case of no applied AC signal and according to [22, 28], Eq. (6) can be solved to get

$$V^{*2}_{\mathrm{gc0}}(x) = V^2_{gs0} - \frac{2I_0}{\beta}x \tag{8}$$

where $\beta = {}^{q}/_{KT}$ and I_0 is the DC channel to source current. Defining

$$y = {}^{x}/_{L_g}\text{, then } V^*_{gc0}(y) = \sqrt{V^2_{gs0} - \frac{2L_gI_0}{\beta}y} = V_{gs0}\sqrt{1-\lambda y} \tag{9}$$

where $\lambda = \frac{2L_gI_0}{\beta V^2_{gs0}} = \frac{I_0}{I_{sat}}$ (in the open drain case, $\lambda = 0$), I_0 is the channel DC current, I_{sat} is the saturation current, $\varepsilon^2 = \frac{V_{gs0}\mu}{\omega L_g{}^2} = \frac{L^2_{eff}}{L_g{}^2}$, and L_{eff} is the effective decay length of the AC signal within the channel.

AC analysis

A realistic FET model must include the effect of multiple AC input signals to its ports., we can define the boundary conditions as:

$$V_{\mathrm{gc}1}(\mathrm{x}=0)=V_{gs1},V_{\mathrm{gc}1}\left(x=L_g\right)=V_{gs1}-V_{ds1}=V_{gd1} \tag{10}$$

$$V_{\mathrm{gc}0}(\mathrm{x}=0)=V_{gs0},V_{\mathrm{gc}0}\left(x=L_g\right)=V_{gs0}-V_{ds0}=V_{gd0} \tag{11}$$

$$\text{Define } g(x)=\frac{V_{\mathrm{gc}0}(x)V_{\mathrm{gc}1}(x)}{V_{gs0}V_{gs1}} \text{ such that } \frac{d^2g(x)}{dx^2}=\frac{i\omega}{\mu}\frac{V_{\mathrm{gc}1}(x)}{V_{\mathrm{gc}0}(x)}$$

$$\text{And } g(0)=1,g(1)=\left(1-\frac{V_{ds0}}{V_{gs0}}\right)\left(1-\frac{V_{ds1}}{V_{gs1}}\right)=\frac{V_{gd0}}{V_{gs0}}\frac{V_{gd1}}{V_{gs1}} \tag{12}$$

From Eq. (9) and based on [22, 28], we get

$$g(y)\simeq c_1(1-\lambda y)^{1/8}exp\left[\frac{4}{3\sqrt{2}}\frac{(i-1)}{\lambda\varepsilon}\left(1-(1-\lambda y)^{3/4}\right)\right]+c_2(1-\lambda y)^{1/8}exp\left[\frac{-4}{3\sqrt{2}}\frac{(i-1)}{\lambda\varepsilon}\left(1-(1-\lambda y)^{3/4}\right)\right] \tag{13}$$

Therefore, we can rewrite the above equation for the open drain case ($\lambda=0$) as

$$g\left(y\right)=c_1exp\left[\frac{(i-1)}{\varepsilon\sqrt{2}}y\right]+c_2exp\left[\frac{(-i+1)}{\varepsilon\sqrt{2}}y\right] \tag{14}$$

$$\text{Let } \alpha=\frac{(1-i)}{\varepsilon\sqrt{2}}=\frac{(i-1)}{\sqrt{2}}\frac{L_g}{L_{eff}}, \text{accordingly } g\left(\mathrm{y}\right)=c_1e^{-\alpha y}+c_2e^{\alpha y} \tag{15}$$

The boundary conditions can be written as

$$g(0)=1, or c_1+c_2=1, \text{and } g(1)=\frac{V_{gd0}}{V_{gs0}}\frac{V_{gd1}}{V_{gs1}} \tag{16}$$

For open drain, $V_{gd0}=V_{gs0}+V_{ds0}\cong V_{gs0}$, and $g(1)\approx\frac{V_{gd1}}{V_{gs1}}=c_3$.

For short channel, $L_g<L_{eff}$, so $|\alpha|<1$. From Eq. (15), we can approximate Eq. (14)

$$\begin{aligned} g\left(\mathrm{y}\right) &= c_1\left(1-\alpha\mathrm{y}\right)+c_2\left(1+\alpha\mathrm{y}\right)\\ &=(c_1+c_2)+(c_1-c_2)\alpha\mathrm{y}\\ &=1-(c_1-c_2)\alpha\mathrm{y}\end{aligned} \tag{17}$$

where $\frac{V_{gd1}}{V_{gs1}}=1-(c_1-c_2)$

DC analysis

Since in open drain case $V_{gc0}\cong V_{gs0}$, the rectification response through the channel $R(x)$ can be expressed as,

$$R(x)=V_{gc0}-\mathrm{V}_{gc0}^{*}\cong\frac{1}{4}\frac{{V_{gs1}}^2}{V_{gs0}}-\frac{g(x)^2{V_{gs1}}^2}{4V_{gs0}}=\frac{{V_{gs1}}^2}{4V_{gs0}}(1-g(x)^2) \tag{18}$$

where V^*_{gc0} is the gate to channel potential at no AC signal applied. For open drain

$$V_{cs1}(x) = V_{gs1} - \frac{g\left(\frac{x}{L_g}\right) V_{gs1} V_{gs0}}{V_{gc0}} \cong V_{gs1} - g\left(\frac{x}{L_g}\right) V_{gs1} \tag{19}$$

We can therefore substitute into Eq. (18) to get the drain response (x = L_g)

$$\begin{aligned} R &= \frac{{V_{gs1}}^2}{4V_{gs0}}(1 - (1 - (c_1 - c_2)\alpha)^2) \\ &= \frac{{V_{gs1}}^2}{4V_{gs0}}(2(c_1 - c_2)\alpha - (c_1 - c_2)^2) = \frac{{V_{gs1}}^2}{4V_{gs0}}\frac{2(c_1 - c_2)L_g}{L_{eff}}(1 - (c_1 - c_2)\frac{L_g}{2L_{eff}}) \end{aligned} \tag{20}$$

In this section, we have shown that in the case of short channel MOSFET the incomplete decay of the AC signal causes incomplete rectification of that signal. Our equations show that an approximately linear relation relates the rectification response to the channel length at very small length, however as the channel length increases the relation deviates from linearity approaching saturation. It is important to identify here that short here is identified with respect to the effective AC decay length of (L_{eff}) which depends both on the frequency as well as the channel parameters itself.

Methods

Our simulated device (Si MOSFET) is defined and structured by Synopsis Sentaurus (TCAD) simulator tool. In the following section, we'll go into more depth on how to model a Si MOSFET to study its ability to detect THz radiation in a short channel.

Device simulation

The device structure of our THz detector is based on N-channel 2D MOSFET. The active device material is silicon. The thickness of the substrate is 7 nm and of the gate oxide (t_{ox}) is 5 nm. Multiple values of gate length were used. The length of the source/drain region is 0.25 µm while the length of the source/drain contact is 0.2 µm. The detector is established with a gate length varied as (L_g= 25,50,60,70,75,100 and 150 nm). Schematic of the device of channel length L_g= 100 nm is shown in Fig. 1.

To operate the MOSFET at open drain mode, the drain current is fixed at zero value. The source and substrate are grounded and THz radiation with frequency (1THz) and amplitude (0.05 V) has been applied to the gate (g). Multiple values of Dc gate voltage (0.1–1.9 V) were simulated. The circuit schematic of the simulated device in this mode is shown in Fig. 2. Two simulation modes were needed, the first one is quasistationary (steady state) mode for dc voltage to extract I-V characteristics and the second is transient where AC signal is applied to the gate with 1THz frequency.

Results

The results of the device characteristics and its simulation results are presented in this section. We extracted also the detailed development of rectified signal within the channel to further study it. The basic characteristics of n MOSFET detector are presented through the well-known I_d- V_d characteristics for FET device in Fig. 3a for $V_g = 6V$ and Fig. 3b for $V_g = 0.5V$ where L_g= (25, 50, 60, 70, 75, 100 and 150 nm).

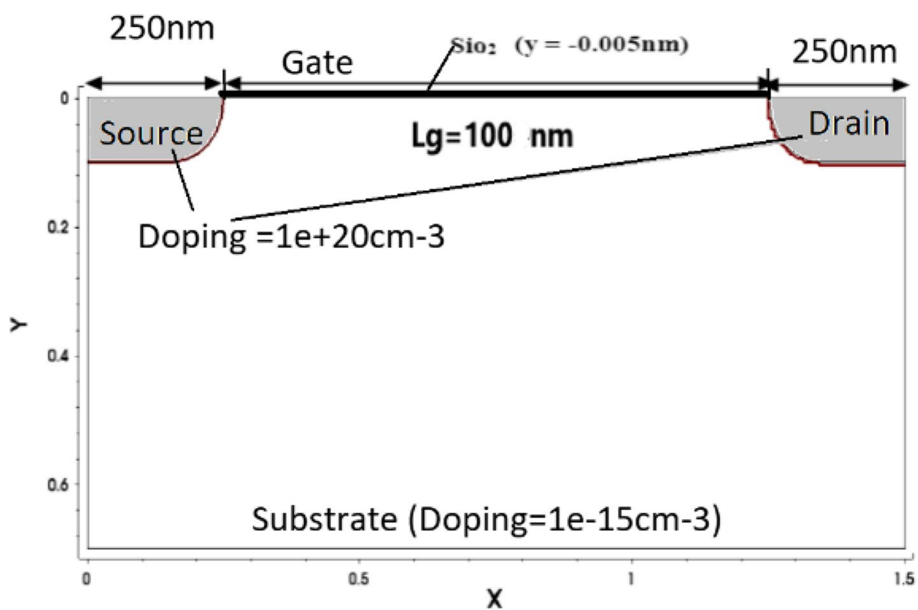

Fig. 1 The structure of the simulated Si MOSFET device

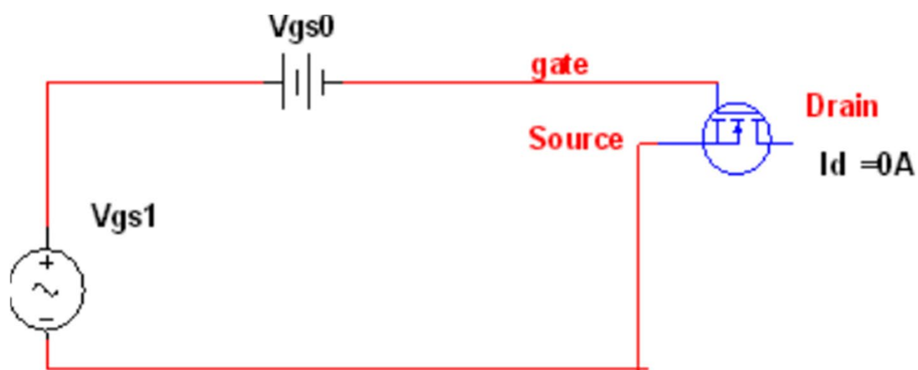

Fig. 2 Circuit model of n MOSFET detector (open drain mode)

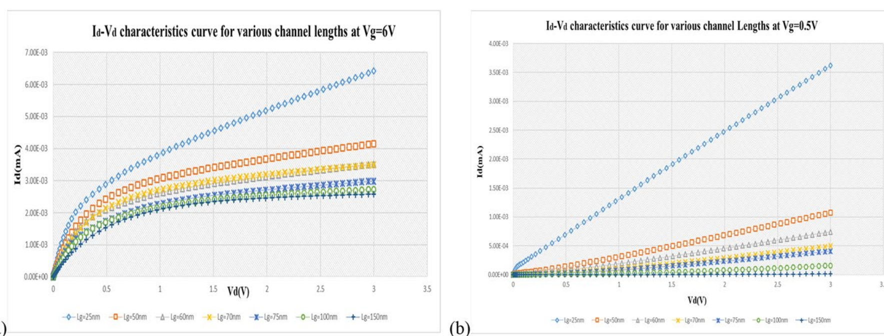

Fig. 3 I_d- V_d curves of simulation of 2D nMOSFET for short channel lengths **a** $Vg = 6$ V and **b** $Vg = 0.5$ V

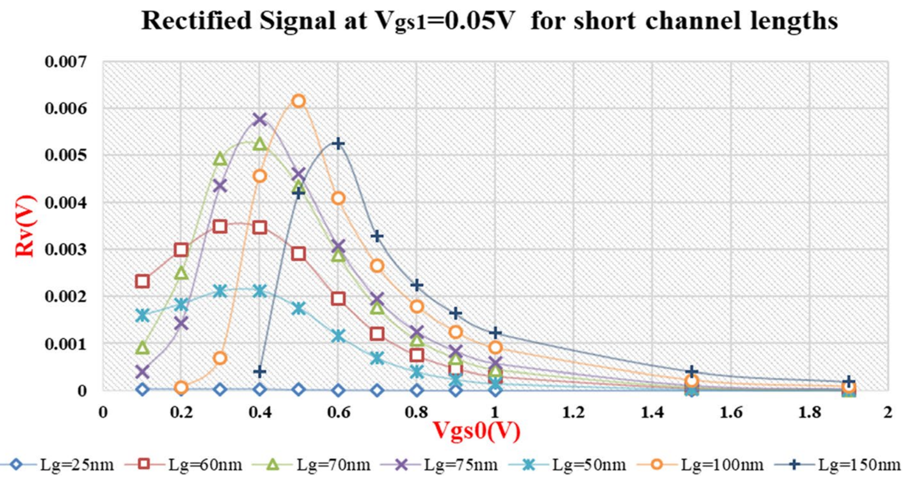

Fig. 4 Rectified drain signal as a function of V_{gs1}

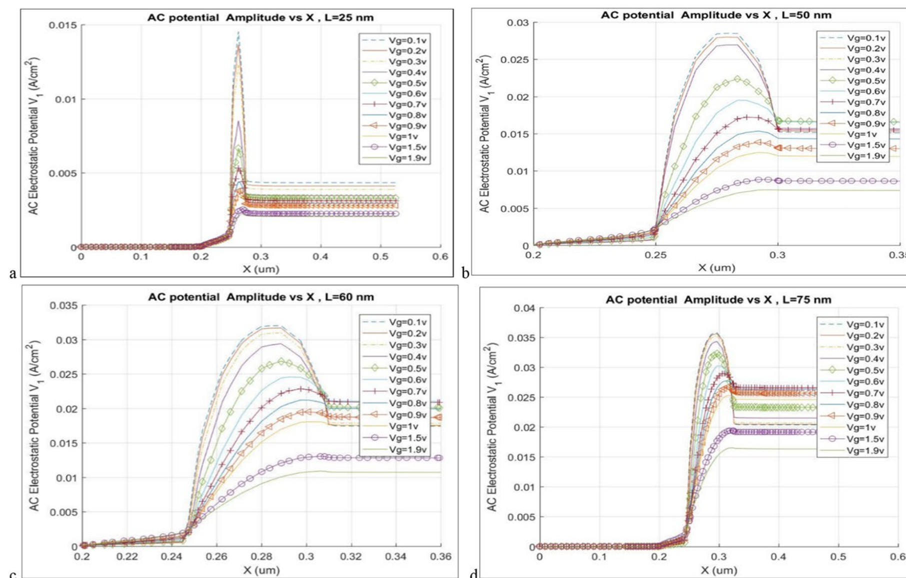

Fig. 5 The AC electrostatic potential amplitude along the channel for **a** Lg = 25 nm, **b** Lg = 50 nm, **c** Lg = 60 nm, and **d** Lg = 75 nm

After extracting the transient output voltage, rectification is calculated from the transient response at a fixed V_{g0}, such as

$$R = \left(\int_0^T V_d(t)|_{V_{g1=0.05}} - V_d|_{V_{g1=0}} dt\right)_{constV_g, L_g, x} \tag{21}$$

At 0.05 V ac amplitude, the rectified signal is obtained in Fig. 4. To analyze these results, we extract the cutlines of the potential along the device channel at the same channel lengths to show the potential profile within the device.

The AC potential across the channel is extracted in Figs. 5 and 7a using Eq. (19) at all channel lengths, the rectified signal inside the channel is illustrated in Figs. 6 and 7b. Finally, in order to verify that discretization in the time step did not give rise to error, we

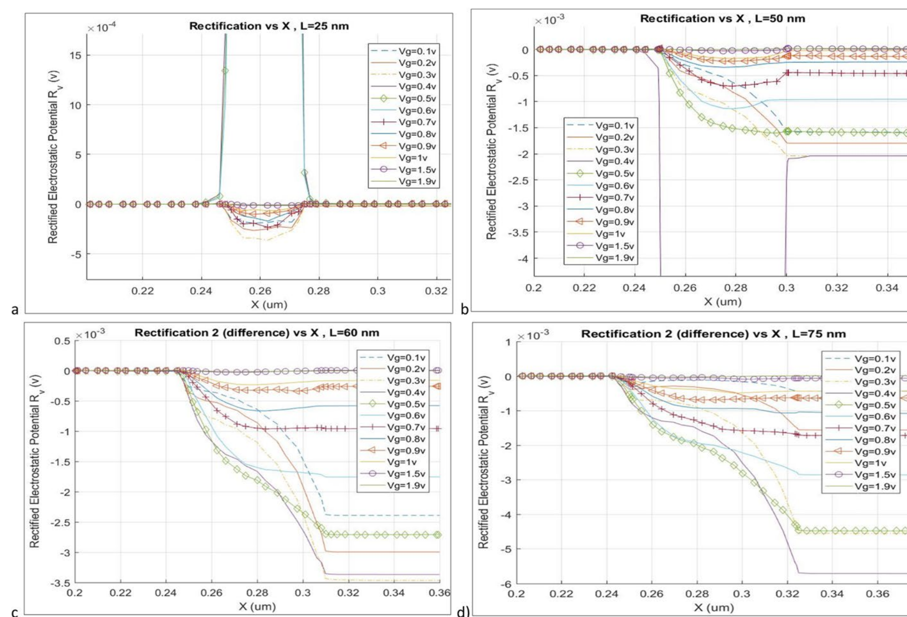

Fig. 6 The rectified potential (R_V) along the channel for **a** Lg = 25 nm, **b** Lg = 50 nm, **c** Lg = 60 nm, and **d** Lg = 75 nm

calculate the rectification of the boundary conditions (especially the drain current) as shown in Fig. 9.

Discussion

To validate the simulation response results which are plotted in Fig. 4, we compare them to experimental data [29]. Figure 8 shows the experimental results of a similar device operation (model of the floating drain with gate AC input) [29], and it exhibits a remarkably high degree of consistency, as both figures show a peak at the threshold potential and a reduced response inversely proportional to the effective gate potential. This is also consistent with the established literature. To account for variation between the manufacture and simulated devices, the normalized response is shown, instead of the exact values, showing consistent behavioral response and an acceptable error percentage of behavioral response and an acceptable error (average deviation) of 0.005.

The discretization error results (Fig. 9) support our expectations ($I_d = 0, V_{g0} = V_{g0}^{*}$), indicating that the data extraction and calculation of the rectification response sufficiency were accurate.

On the other hand, the dependence of R_{max} requires analyzing the AC potential first. As shown in the last section, the absorption of AC signal within the channel is related to the channel length. In order to explicate this effect, we compare between the rectification response (Fig. 4) and the theoretical response in the model developed in Theoretical analysis section. The change of AC signal through the channel is shown in Figs. 5 and 7a showing incomplete decay of the AC signal due to the short channel lengths.

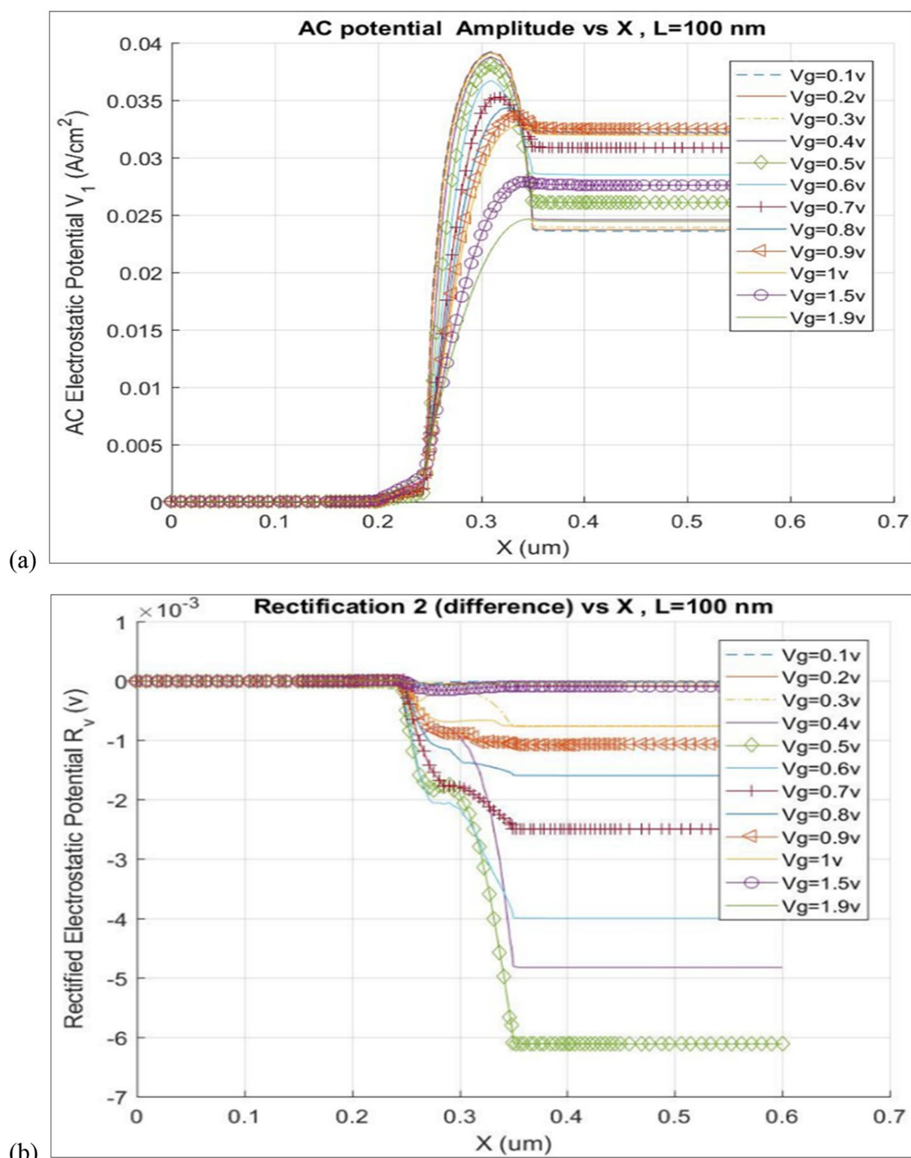

Fig. 7 **a** The AC electrostatic amplitude and **b** the rectified potential response along the channel (Lg = 100 nm)

Increasing the channel length causes almost complete decay of the AC decay through the channel. The Ac amplitude at the source is fixed at 0 (V_{gs1}= 0.05 V) while the AC signal at the drain is determined by both the decayed component through the channel as well as the drain stray capacitances which are affected by the gate potential.

The results of rectification response at varying channel lengths (Fig. 4) show that the peak response varies both in value (R_{max}) and in the corresponding gate potential (V_{gmax}). The change in V_{gmax} is due to the shift in threshold potential due to varying the channel length. This dependence can be shown in Fig. 10 where both V_{th} and V_{gmax} are plotted at varying in channel length. The dependence of the rectification response on the AC amplitude at the terminals is presented in Eq. (18) through ($V_{gs1}{}^2 - V_{gd1}{}^2$) while Eq. (20) shows the dependence of this AC differential on the channel length for

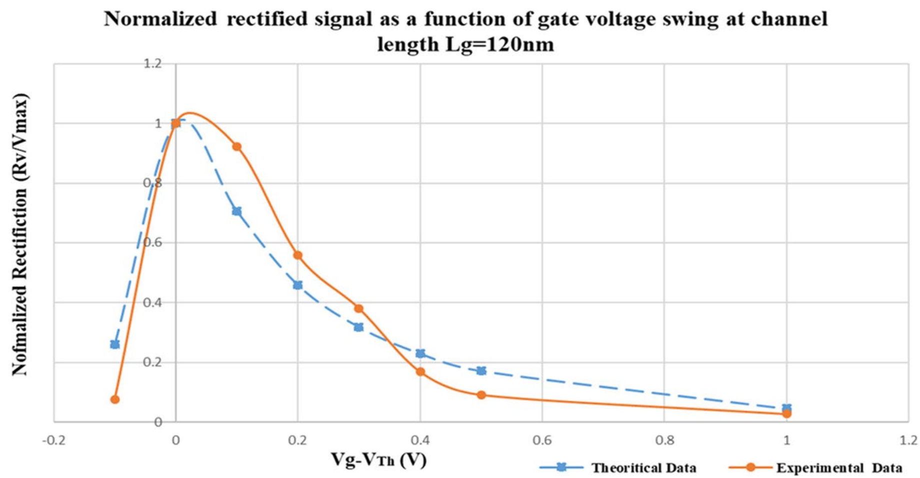

Fig. 8 Theoretical (dash line) and experimental [29] (solid line) response of the nMOSFET vs effective DC gate voltage ($V_{gs0} - V_{th}$)

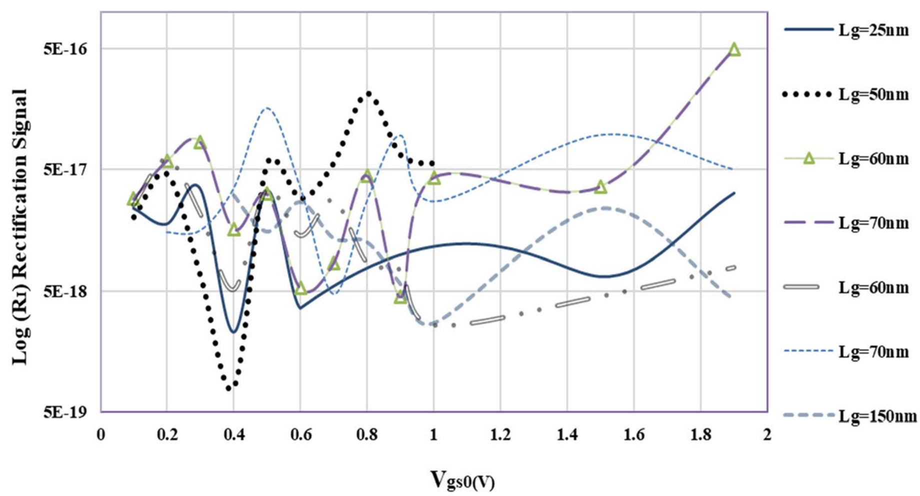

Fig. 9 The discretization error at different values of V_{gso}

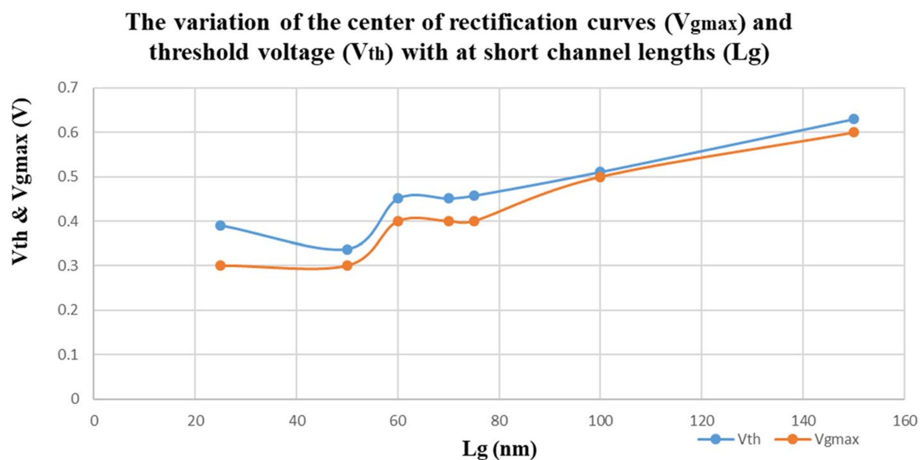

Fig. 10 The variation of both V_{th} and V_{gmax} with channel length (L_g)

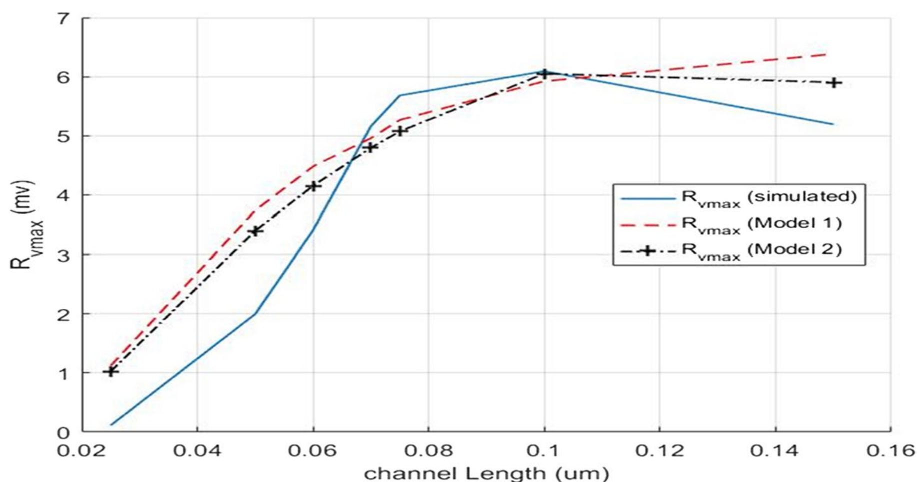

Fig. 11 The variation of R_{max} with channel length L_g

($L_g < L_{eff}$). The results of this model are plotted versus the maximum response R_{max} from the TCAD simulation. Figure 11 shows the R_{max} vs channel length and the dependence of (V_{gs1}^2-V_{gd1}^2) where V_{gs1}&V_{gd1} are extracted from the simulation results given in Figs. 5 and 7a. This figure also shows Eq. (13) where h_0 is chosen as the best fit parameter.

The results shown in Fig. 11 indicated the accuracy of Eq. (20) showing the initial dependence of the rectification response on the channel length. This dependence tends to saturate as the channel length reaches the AC decay length L_{eff}.

Conclusions

A physics-based model as well as a TCAD simulation study of a Si MOSFET with a short channel length acting as a THz detector are presented in this paper. Our model proposes that decreasing the channel length below the effective decay length of the THz signal causes incomplete signal decay and rectification. Our model was able to extract and formulate this effect analytically and show it through TCAD simulation as well across a wide range of gate bias voltages. The observed results are consistent with the analytical model that we have developed. In addition, this study shows a detailed buildup of the rectification through the channel of the MOSFET which we argue is a significant tool for understanding the modeling of FET THz detectors. However, the simulation results show that expanding this study to include increasing channel length is important to investigate any damping effects around and beyond the effective decay length. Increasing the channel length beyond the effective decay length shouldn't affect the rectification by variations in terminal AC signals as they saturate at a maximum value however a detailed study is required to investigate other dependencies.

As a result of the current low efficiency of THz FET detectors, attempts are ongoing to explore the limits of the device performance and their dependence of the different parameters of its design. The results presented here provide an important criterion to optimize the device design and response, which is the minimum channel length at which the device is ineffective for THz detection. They also identify the relation between the optimum operation frequency, channel length, and rectification response.

Abbreviations

Si MOSFET	Silicon metal oxide semiconductor field effect transistor
HEMT	High electron mobility transistor
TCAD	Technology computer-aided design
STDF	Science, Technology & Innovation Funding Authority

Acknowledgements
The authors thankfully acknowledge the Science, Technology & Innovation Funding Authority for its funding and support.

Authors' contributions
YA and NY contributed to the design of the model and analyzed the data simulations. YA and NY aided in interpreting the results and worked on the manuscript. YA carried out the model simulations, designed the figures, and wrote the manuscript in consultation with NY. Both MY and SE contributed to the final version of the manuscript and supervised the work. The author(s) read and approved the final manuscript.

Funding
This work was funded by STDF, "Science, Technology & Innovation Funding Authority," and funding project number (25696).

Availability of data and materials
The datasets used and/or analyzed during the current study are available from the corresponding author upon reasonable request.

Declarations

Competing interests
The authors declare that they have no competing interests.

Received: 21 February 2023 Accepted: 31 March 2023
Published online: 05 May 2023

References

1. Kim S, Park D-W, Choi K-Y, Lee S-G (2015) MOSFET characteristics for terahertz detector application from on-wafer measurement. IEEE Trans Terahertz Sci Technol 5(6):1068–1077. https://doi.org/10.1109/TTHZ.2015.2487780
2. Pala N, Teppe F, Veksler D, Deng Y, Shur MS, Gaska R (2005) Nonresonant detection of terahertz radiation by silicon-on-insulator MOSFETs. Electron Lett 41(7):447. https://doi.org/10.1049/el:20058182
3. Tauk R et al (2006) Plasma wave detection of terahertz radiation by silicon field effects transistors: responsivity and noise equivalent power. Appl Phys Lett 89(25):253511. https://doi.org/10.1063/1.2410215
4. But D (2014) Silicon based terahertz radiation detectors. In: Charles Coulomb Lab. – UMR 5221 CNRS-Univ. Montp. 2, p 104
5. Shang D, Xing Y, Sun P (2019) Short-channel MOSFET for terahertz wave detection fabricated in 55 nm silicon CMOS process technology. Electron Lett 55(25):1357–1358. https://doi.org/10.1049/el.2019.2879
6. Delgado Notario JA et al (2017) Experimental and theoretical studies of Sub-THz detection using strained-Si FETs. J Phys Conf Ser 906:012003. https://doi.org/10.1088/1742-6596/906/1/012003
7. Knap W et al (2010) Field effect transistors for terahertz detection – silicon versus III–V material issue. Opto—Electron Rev 18(3):225–230. https://doi.org/10.2478/s11772-010-018-7
8. Ludwig F, Bauer M, Lisauskas A, Roskos HG (2019) Circuit-based hydrodynamic modeling of AlGaN/GaN HEMTs. In: ESSDERC 2019 - 49th European Solid-State Device Research Conference (ESSDERC), Cracow, Poland, pp 270–273. https://doi.org/10.1109/ESSDERC.2019.8901683
9. Bauer M et al (2019) A high-sensitivity AlGaN/GaN HEMT terahertz detector with integrated broadband bow-tie antenna. IEEE Trans Terahertz Sci Technol 9(4):430–444. https://doi.org/10.1109/TTHZ.2019.2917782
10. Kim S, Hong S, Jang J (2020) Strong and narrowband terahertz radiation from GaAs based pHEMT and terahertz imaging. Microw Opt Technol Lett 62(12):3791–3795. https://doi.org/10.1002/mop.32525
11. Hassanalieragh M, Newman JD, Fourspring K, Ignjatovic Z (2017) THz detection in sub-threshold Si MOSFETs by non-linear channel electron density modulation. In: 2017 IEEE 60th International Midwest Symposium on Circuits and Systems (MWSCAS), Boston, MA, USA, pp 1434–1437. https://doi.org/10.1109/MWSCAS.2017.8053202
12. Horowitz JD (2017) Characterization of optimized Si-MOSFETs for terahertz detection. RIT Scholar Works, Rochester Institute of Technology
13. Wang J, Du G, Liu X (2015) Monte Carlo investigation of Silicon MOSFET for terahertz detection. In: 2015 International Conference on Simulation of Semiconductor Processes and Devices (SISPAD), Washington, DC, pp 210–213. https://doi.org/10.1109/SISPAD.2015.7292296
14. Ikamas K, Nevinskas I, Krotkus A, Lisauskas A (2018) Silicon field effect transistor as the nonlinear detector for terahertz autocorellators. Sensors 18(11):3735. https://doi.org/10.3390/s18113735
15. Ibrahim NY, Rafat NH, Elnahwy SEA (2013) Modeling of field effect transistor channel as a nonlinear transmission line for terahertz detection. J Infrared Millim Terahertz Waves 34(10):606–616. https://doi.org/10.1007/s10762-013-0009-0
16. Dyakonov M, Shur M (1996) Detection, mixing, and frequency multiplication of terahertz radiation by two-dimensional electronic fluid. IEEE Trans Electron Devices 43(3):380–387. https://doi.org/10.1109/16.485650

17. Lisauskas A, Pfeiffer U, Öjefors E, Bolìvar PH, Glaab D, Roskos HG Rational design of high-responsivity detectors of terahertz radiation based on distributed self-mixing in silicon field-effect transistors. J Appl Phys. 105(11). https://aip.scitation.org/doi/10.1063/1.3140611. Accessed 5 Feb 2022
18. Ayoub AB, Ibrahim NY, Elnahwy SEA (2020) Second-order non-quasi-static, compact model of field-effect transistor revealing terminal rectification beyond their cutoff frequency. IET Circuits Devices Syst 14(5):660–666. https://doi.org/10.1049/iet-cds.2019.0127
19. Gutin A, Nahar S, Hella M, Shur M (2013) Modeling terahertz plasmonic Si FETs with SPICE. IEEE Trans Terahertz Sci Technol 3(5):545–549. https://doi.org/10.1109/TTHZ.2013.2262799
20. Gutin A, Ytterdal T, Kachorovskii V, Muraviev A, Shur M (2013) THz SPICE for modeling detectors and nonquadratic response at large input signal. IEEE Sens J 13(1):9
21. Sakhno M, Golenkov A, Sizov F (2013) Uncooled detector challenges: Millimeter-wave and terahertz long channel field effect transistor and Schottky barrier diode detectors. J Appl Phys 114(16):164503. https://doi.org/10.1063/1.4826364
22. Ibrahim NY, Rafat NH, Elnahwy SEA (2015) Drift transport model of field effect transistors in saturation beyond cutoff. J Phys Appl Phys 48(13):135102. https://doi.org/10.1088/0022-3727/48/13/135102
23. Elkhatib TA, Kachorovskii VYu, Stillman WJ, Rumyantsev S, Zhang X-C, Shur MS (2011) Terahertz response of field-effect transistors in saturation regime. Appl Phys Lett 98(24):243505. https://doi.org/10.1063/1.3584137
24. Ibrahim NY, Rafat NH, Elnahwy SEA (2015) Multi-input intrinsic and extrinsic field effect transistor models beyond cutoff frequency. Solid-State Electron 103:236–241. https://doi.org/10.1016/j.sse.2014.07.006
25. Gutin A, Kachorovskii V, Muraviev A, Shur M (2012) Plasmonic terahertz detector response at high intensities. J Appl Phys 112(1):014508. https://doi.org/10.1063/1.4732138
26. Ibrahim N, Rafat NH, El-Din Elnahwy S (2016) Simulation study for the use of transistor contacts for sub-terahertz radiation detection. IET Microw Antennas Propag 10(7):784–790. https://doi.org/10.1049/iet-map.2015.0492
27. Sze SM, Lee MK (2012) Semiconductor devices, physics and technology, 3rd edn. Wiley, Hoboken
28. Ibrahim NYM (2014) Modeling terahertz radiation detection using field effect transistors beyond cutoff. Cairo University, Faculty of Engineering, p 147
29. Khan MIW, Kim S, Park D-W, Kim H-J, Han S-K, Lee S-G (2018) Nonlinear analysis of nonresonant THz response of MOSFET and implementation of a high-responsivity cross-coupled THz detector. IEEE Trans Terahertz Sci Technol 8(1):108–120. https://doi.org/10.1109/TTHZ.2017.2778499

Publisher's Note

Springer Nature remains neutral with regard to jurisdictional claims in published maps and institutional affiliations.

Submit your manuscript to a SpringerOpen journal and benefit from:

- Convenient online submission
- Rigorous peer review
- Open access: articles freely available online
- High visibility within the field
- Retaining the copyright to your article

Submit your next manuscript at ▶ springeropen.com